Chemical Science

EDGE ARTICLE

View Article Online
View Journal | View Issue

Cite this: *Chem. Sci.*, 2019, **10**, 10025

All publication charges for this article have been paid for by the Royal Society of Chemistry

Internal acidity scale and reactivity evaluation of chiral phosphoric acids with different 3,3′-substituents in Brønsted acid catalysis†

Kerstin Rothermel, Maxime Melikian, Johnny Hioe, Julian Greindl, Johannes Gramüller, Matej Žabka, Nils Sorgenfrei, Thomas Hausler, Fabio Morana and Ruth M. Gschwind *

The concept of hydrogen bonding for enhancing substrate binding and controlling selectivity and reactivity is central in catalysis. However, the properties of these key hydrogen bonds and their catalyst-dependent variations are extremely difficult to determine directly by experiments. Here, for the first time the hydrogen bond properties of a whole series of BINOL-derived chiral phosphoric acid (CPA) catalysts in their substrate complexes with various imines were investigated to derive the influence of different 3,3′-substituents on the acidity and reactivity. NMR ^{1}H and ^{15}N chemical shifts and $^{1}J_{NH}$ coupling constants of these hydrogen bonds were used to establish an internal acidity scale corroborated by calculations. Deviations from calculated external acidities reveal the importance of intermolecular interactions for this key feature of CPAs. For CPAs with similarly sized binding pockets, a correlation of reactivity and hydrogen bond strengths of the catalyst was found. A catalyst with a very small binding pocket showed significantly reduced reactivities. Therefore, NMR isomerization kinetics, population and chemical shift analyses of binary and ternary complexes as well as reaction kinetics were performed to address the steps of the transfer hydrogenation influencing the overall reaction rate. The results of CPAs with different 3,3′-substituents show a delicate balance between the isomerization and the ternary complex formation to be rate-determining. For CPAs with an identical acidic motif and similar sterics, reactivity and internal acidity correlated inversely. In cases where higher sterical demand within the binary complex hinders the binding of the second substrate, the correlation between acidity and reactivity breaks down.

Received 14th May 2019
Accepted 2nd September 2019

DOI: 10.1039/c9sc02342a

rsc.li/chemical-science

Introduction

Over the past decade, a large number of reactions were developed, where enantioenriched products are formed using a chiral organic molecule with acidic functionality as catalyst.[1–3] A prominent example of the so-called chiral Brønsted acid catalysis was a Strecker reaction catalyzed by peptide-based thiourea derivatives.[1,4–6] One success factor of Brønsted acid catalysts in enantioselective transformations is the formation of a central hydrogen bond between catalyst and substrate, thus anchoring the structures, which favor one enantiotopic face over the other.[1] Another milestone was the development of chiral phosphoric acid (CPAs) catalysts with BINOL (1,1′-bi-2-naphthol) backbones by Akiyama and Terada.[7,8] These catalysts are applicable in several highly enantioselective reactions with imines such as transfer hydrogenations,[9–11] reductive aminations,[12,13] Mannich-type reactions[14–16] and Strecker reactions.[17] In particular, in the asymmetric reduction of imines with Hantzsch 1,4-dihydropyridine ester, these BINOL derived CPAs can achieve high yields as well as high enantioselectivities.[12,18–20]

Rueping *et al.* proposed a catalytic cycle (Fig. 1a), where the imine is protonated by the phosphoric acid and forms a hydrogen bond assisted ion pair (step A).[18] In the next step, the thermodynamically more stable *E*-imine is isomerized to the minor-populated *Z*-imine complex (step B). Calculations as well as our previous experimental study showed that the transition state of the Z-imine complex is energetically more favoured.[21] Then, the Hantzsch ester approaches and a ternary complex is formed (step C). In the last step, the hydride transfer from the Hantzsch ester (step D) leads to the chiral amine (step E), while the pyridinium salt regenerates the Brønsted acid.[18]

This asymmetric reduction of imines works with many different CPAs, which differ only in the 3,3′-substituents. Prominent examples are amongst others TRIP (3,3′-bis(2,4,6-triisopropylphenyl)-1,1′-binaphthyl-2,2′-diyl hydrogen phosphate), TRIFP (3,3′-bis(3,5-bis(trifluoromethyl)phenyl)-1,1′-

Institut für Organische Chemie, Universität Regensburg, Universitätsstraße 31, D-93053 Regensburg, Germany. E-mail: ruth.gschwind@chemie.uni-regensburg.de

† Electronic supplementary information (ESI) available. See DOI: 10.1039/c9sc02342a

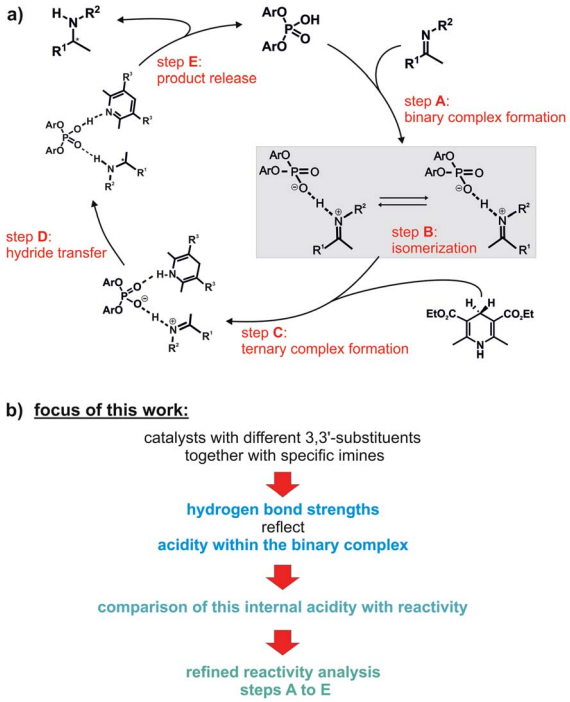

Fig. 1 (a) Proposed catalytic cycle for the asymmetric transfer hydrogenation with CPAs;[18] (b) the influence of different 3,3′-substituents of the catalyst on the hydrogen bond of the ion pair (highlighted in grey) was investigated. In addition, the effect of the varying internal acidities of the binary complexes on the overall reaction rate of the shown transfer hydrogenation was the focus of this work.

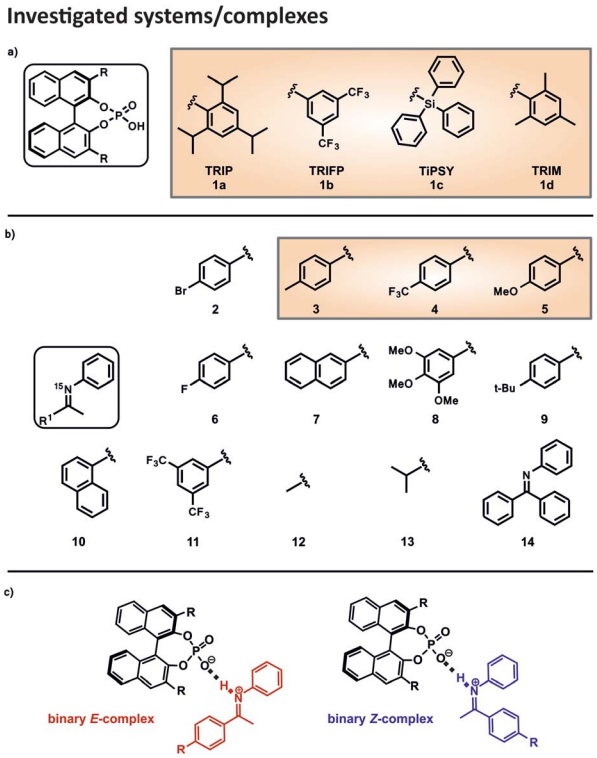

Fig. 2 Structures of the investigated (a) phosphoric acids with different 3,3′-substituents and (b) imines. The hydrogen bonds of the binary complexes of TRIP **1a**, TRIFP **1b**, TiPSY **1c** and TRIM **1d** with the imines **3**, **4** and **5** were investigated in detail by means of NMR. The other imines **2** and **6–13** are necessary to cover the complete hydrogen bond range of the Steiner–Limbach curve. The non-isomerizable imine **14** was used to investigate the influence of the Hantzsch ester concentration on the reaction rate. (c) The main focus of this work was the NMR-spectroscopic investigation of the binary CPA/imine-complexes. The imine exists either as *E*- or *Z* isomer.

binaphthyl-2,2′-diyl hydrogen phosphate) and TiPSY (3,3′-bis(triphenylsilyl)-1,1′-binaphthyl-2,2′-diyl hydrogen phosphate) (Fig. 2a).[18,19,22] Thus, the 3,3′-substituents are the key to ee values and yields and sometimes even reverse stereoselectivity.[23–26] The way that structures of the catalysts influence the outcome varies from reaction to reaction and, up to now, there have been few direct experimental measurements of relevant structural features.[27] Thus, the screening of the catalysts to find the most effective BINOL-derived CPA is still the predominantly employed method in synthesis. On the contrary, *in silico*, the understanding of the occurring interactions and structures is by far more developed.[28] One approach follows a multivariate regression model analysis, utilizing various parameters to develop a mathematical model that explains the relationship between structure and reactivity or selectivity. This model is capable of distinguishing certain crucial non-covalent interactions present between the catalyst and the substrate.[29,30]

In 2016, Goodman *et al.* introduced some parameters to describe the steric bulk of the 3,3′-substituents of the catalysts. Thus, they could show that the stereoselectivity of the asymmetric transfer hydrogenation of imines (Fig. 1a) is widely dependent on two parameters: the rotation barrier describing the proximal bulk and the AREA (θ) taking the distal bulk into account.[31] Also, other groups investigated the influence of different 3,3′-substituents of CPAs in several reactions regarding the occurring transition states, the structural differences and/or the enantioselectivity by theoretical methods.[32–40]

Nevertheless, our recent NMR study about the influence of 3,3′ substituents on the structures and populations of binary CPA/imine complexes revealed a significant deviation of experimental populations compared to those calculated with the standard theoretical methods applied to these systems.[41] In general, experimental insight into the structures involved in Brønsted acid catalysis is very rare.[42,43] In earlier studies we revealed the hydrogen bond strengths and geometries of TRIP/imine complexes in detail.[42] In addition, we could experimentally show that for TRIP, TRIFP, TiPSY and TRIM (3,3′-bis(2,4,6-trimethylphenyl)-1,1′-binaph-thyl-2,2′-diyl hydrogen phosphate) four different core structures of their binary CPA/imine complexes are omnipresent in solution (*Type I/II E* and *Type I/II Z*).[41,43] The different 3,3′-substituents influence mainly the energetics/population of these binary complexes, however, much less their general sterically features and interaction patterns.[41] Nevertheless, despite the crucial function of hydrogen bonds in Brønsted acid catalysis as structural anchor[43] or regarding acidity/reactivity correlations[44] detailed experimental insights about the effect of 3,3′ substituents on this hydrogen bond are elusive so far.

In general, the formation of hydrogen bonds in catalyst/substrate complexes is often highly relevant and plays a key role in the activation of the substrate. For example, in the field of asymmetric catalysis, the activation of electrophilic substrates such as carbonyls or imines seems to take place *via* a hydrogen bond.[3,9,45,46] Also in photochemistry several examples are known, where the proposed mechanisms is based on a hydrogen-bonded species. For example, Knowles *et al.* could show that ketones, amides or alcohols can be converted by a proton-coupled electron transfer (PCET) and assumed hydrogen bond formation between the substrate and proton donor/acceptor prior to the electron transfer.[47–49] Finally, there are various examples throughout organocatalysis, in which the substrate binding and activation *via* a hydrogen bonded species is proposed.[50–54] However, the central hydrogen-bonded species are often in fast chemical exchange or have short lifetimes, therefore it is for most of the systems experimentally not possible to detect these hydrogen bonds.

In the literature, hydrogen bonds are described as the start of a proton transfer reaction.[55,56] This means that the position of the proton inside the hydrogen bond varies depending on the acidity of the hydrogen bond donor respectively basicity of the acceptor. Limbach *et al.* developed on model systems a NMR spectroscopic access to the position of these hydrogen atoms inside the hydrogen bonds using an empirical correlation of the ^{1}H and the ^{15}N chemical shifts.[57,58] This in combination with our recently developed access to the hydrogen bonds in CPA/imine complexes[42] allows for the first time to tackle the effect of the 3,3′-substituent on the hydrogen bonds and thus on the acidity of the CPAs within the binary complex with NMR. This acidity may play a crucial role regarding reactivity. However, up to now there are only few experimentally determined pK_a values of CPAs. In 2011, O'Donoghue *et al.* determined pK_a values for TRIP and TRIFP in DMSO by using a spectrophotometric titration method.[59,60] Here, variations of the 3,3′-substitents resulted in modulation of the pK_a-values of the CPAs up to ~1.5 pK_a units (pK_{aTRIP} (DMSO) = 4.22 and pK_{aTRIFP} (DMSO) = 2.63).[60] In acetonitrile, a similar variation range of experimental pK_a values for five phosphoric acids between 12.5 and 14.0 is found (pK_{aTRIP} (ACN) = 13.3).[44] However, BINOL-derived *N*-triflylphosphoramides show significant smaller pK_a values between 6.3 and 6.9.[44] Thus, at least in acetonitrile, the acidity of the catalysts is significantly influenced by the acidic motif, while the 3,3′-substituents have minor effects.[44] Most interestingly, in a Nazarov cyclization higher rates were found for more acidic Brønsted acids and a direct correlation between acidity and reactivity was postulated.[44] Given the large deviations of CPA acidities between the previous studies and our access to hydrogen bonds in CPA imine complexes for TRIP this opens up the possibility to measure an internal acidity scale of the catalysts. Furthermore, this internal acidity analysis is of central interest for a reactivity analysis, because the acidity potentially influences any step in the catalytic cycle (see steps A to E in Fig. 1a).

Therefore, in this study, we used four CPAs with different 3,3′-substituents and several imines to develop for the first time an internal acidity scale for binary CPA/imine complexes. This scale is based on chemical shifts and $^{1}J_{NH}$ coupling constants of the binary complexes obtained by NMR at low temperatures. The resulting internal acidities of the catalysts were compared with their respective reactivity in the transfer hydrogenation. In addition, a multitude of experimental and theoretical data was used to identify the reaction steps contributing to the overall reaction rate.

Results and discussion

Investigated systems/complexes

In order to investigate the influence of different 3,3′-substituents on the acidity of CPAs and to correlate this internal acidity with the reactivity in transfer hydrogenations, we selected four different CPAs and twelve imines with different electronic and steric properties (Fig. 2). The binary complexes of the four CPAs **1a–1d** with the imines **2** and **6–13** were used to cover the whole range of the Steiner–Limbach curve, while imines **3**, **4** and **5** were chosen for a detailed hydrogen bond analysis within the binary complexes. Altogether, we screened 32 different binary complexes. ^{15}N labelling of the imines allowed the access to the ^{15}N chemical shifts[42] and CD_2Cl_2 was chosen as solvent, since CD_2Cl_2 provides the best chemical shift dispersion and smallest line widths of all solvents investigated. To reach the slow exchange regime of the hydrogen bonds all spectra were recorded at 180 K unless otherwise mentioned.

Determination of the internal acidity of the CPAs

Since external pK_a measurements/calculations are performed *versus* protons, whereas in the transfer hydrogenation a binding to an imine occurs, there is no reason why there necessarily should be a correlation between external acidity and reactivity. Therefore, an internal acidity scale for the CPAs was constructed within the binary CPA imine complexes to be later compared to the reactivity. The Steiner–Limbach correlation can be used to characterize hydrogen bonds in phosphoric acid catalyst/imine complexes as previously demonstrated for TRIP/imine complexes.[42] By plotting the ^{1}H chemical shift $\delta_{(OHN)}$ of the acidic proton against the ^{15}N chemical shift $\delta_{(OHN)}$ of the basic nitrogen, a parabolic correlation curve can be fitted through the data points (see Fig. 3 and ESI† Chapter 3). All CPA/imine complexes investigated in this work feature a strong hydrogen bond with ^{1}H chemical shifts ranging from 15 to 19 ppm (see highlighted points in Fig. 3a). Their referenced ^{15}N chemical shifts (for details see ESI† Chapter 3.2) range from −90 to −150 ppm. Furthermore, for many of these binary complexes magnetisation transfers across the hydrogen bond *via* $^{3h}J_{PN}$ and $^{2h}J_{PH}$ are detectable. All of these parameters are typical for a strong hydrogen bond with a substantial covalent character providing high geometrical preferences for a linear arrangement. The position of these binary complexes on the left side of the curve (highlighted in Fig. 3a) shows that these binary complexes have a partial ion pair character.

Since in the first step of the asymmetric transfer hydrogenation the activation of the imine *via* a hydrogen bond formation is assumed (Fig. 1a), this hydrogen bond of the binary complex can be used to monitor the binding between catalyst and substrate. In general, three parameters can be used to

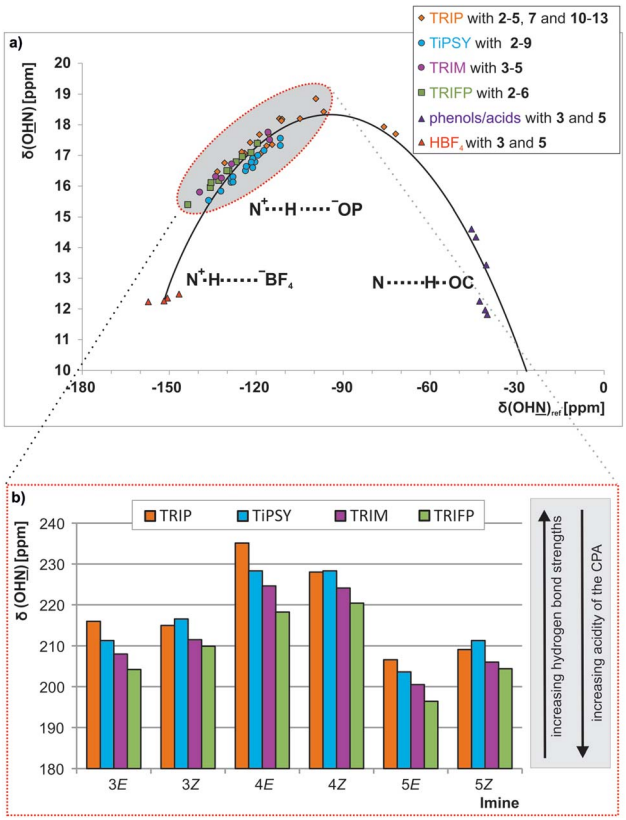

Fig. 3 (a) In the Steiner–Limbach curve the $\delta_{(OHN)}$ is plotted *versus* $\delta_{(OHN)}$ of the hydrogen bonded complexes. All CPA/imine complexes are located on the left side of the curve (highlighted in grey) and form hydrogen-bond assisted ion pairs. The data for the complexes with TRIP, HBF_4, phenols and carboxylic acids were taken from ref. 42 All ^{15}N chemical shifts are referenced to $\{\delta(OHN)_{ref} = \delta(OHN)_{exp} - 340$ ppm$\}$ (for details and exact values see ESI† Chapter 3); (b) the experimental δ(OHN) of the imines **3**, **4** and **5** in the binary complexes with the CPAs **1a–1d** are shown.

determine the hydrogen bond strength: the chemical shifts of ^1H and ^{15}N as well as the $^1J_{NH}$ coupling constants. While the ^1H chemical shift is known to be significantly influenced by anisotropic shielding effects *e.g.* from aromatic moieties and other neighbourhood effects, the ^{15}N chemical shift of TRIP/imine complexes was shown to reflect directly the hydrogen bond situation.[42] Therefore, the ^{15}N chemical shift was used as a descriptor for the hydrogen bond strength and acidity of the catalyst, which also directly correlates with the $^1J_{NH}$ coupling constant (see discussion below).

Internal acidity: chemical shift analysis

The encircled area in the Steiner–Limbach curve in Fig. 3a and the corresponding graph in Fig. 3b, representing complexes with imines **3**, **4** and **5**, reveal different hydrogen bond strengths for the four catalysts and common trends for *E*- and *Z*-imines (for details see ESI† Chapter 3.6). In general, for all CPA/*Z*-imine complexes stronger hydrogen bonds are observed than for the complexes with *E*-imines, as indicated by the low field shift of the hydrogen atom as well as the nitrogen atom. Due to the reduced steric requirements of the imine in the *Z*-configuration the imine can approach closer to the catalyst. This is corroborated by the experimentally derived atomic distances of the hydrogen bonds of the TRIP complexes[42] and further supported by the distances in the calculated structures of various binary complexes (for coordinates see ESI† Chapter 17). Furthermore, within the *E*- and *Z*-complexes different trends regarding the hydrogen bond strengths upon variation of the catalyst are observed: for the *E*-complexes TRIP forms the strongest hydrogen bonds (least negative ^{15}N chemical shift), followed by TiPSY, TRIM and TRIFP. For *Z*-complexes TiPSY forms the strongest hydrogen bond directly followed by TRIP and then with a slight gap again followed by TRIM and TRIFP. These trends of the hydrogen bond strengths (TRIP > TiPSY > TRIM > TRIFP for *E*-complexes and TiPSY ≥ TRIP > TRIM > TRIFP for *Z*-complexes) were observed for imines **3–5** and could be confirmed by the $^1J_{NH}$ coupling constants (see below). The hydrogen bond strengths can be directly correlated with the internal acidity of the CPA,[61] because with a given imine a variation of the acidity of the catalyst changes the position of the proton in the hydrogen bond. In case of the investigated hydrogen assisted ion pair complexes, which are located on the left side of the Steiner–Limbach curve, a higher acidity effects a weaker hydrogen bond. That means a higher acidity or lower pK_a value of the CPA relates to a reduced ^1H and ^{15}N chemical shift (larger negative value for the referenced ^{15}N) and an increased $^1J_{NH}$ coupling constant. In summary, the chemical shift analysis yielded two different internal acidity scales, *i.e.* scales for the binary *E*-complexes ($pK_{aTRIP} > pK_{aTiPSY} > pK_{aTRIM} > pK_{aTRIFP}$) and the *Z*-complexes ($pK_{aTiPSY} \geq pK_{aTRIP} > pK_{aTRIM} > pK_{aTRIFP}$).

Internal acidity: $^1J_{NH}$ coupling constants analysis

The analysis of the $^1J_{NH}$ coupling constants (Fig. 4) confirms the internal acidity of the catalyst for both *E*- and *Z*-complexes. Furthermore, the Hammett σ_{para} values of the aryl substituents of the imines correlate with the coupling constants for *E*- and *Z*-complexes of imine **3–6** (see ESI† Chapter 5). Given the fact that the hydrogen bond of all investigated CPA/imine complexes tends towards ionic complexes, *i.e.* to a complete proton transfer, lower $^1J_{NH}$ coupling constants correspond to stronger hydrogen bonds. Within all investigated CPA/*E*-imine complexes TRIP shows the smallest $^1J_{NH}$ coupling constants, followed by TiPSY, TRIM and TRIFP. This is in accordance with the internal acidities ($pK_{aTRIP} > pK_{aTiPSY} > pK_{aTRIM} > pK_{aTRIFP}$) discussed before based on the ^{15}N chemical shifts. For the *Z*-complexes, in almost all cases slightly smaller $^1J_{NH}$ coupling constants than for *E*-complexes were observed, corroborating the stronger hydrogen bonds derived from the chemical shift analysis (see above). For the CPA/*Z*-imine complexes $^1J_{NH}$ coupling constants for TiPSY are slightly smaller than for TRIP, suggesting stronger hydrogen bond and shorter distance from the catalyst, thus congesting the active catalyst pocket (Fig. 4).

In our theoretical calculations, the same qualitative trend for the scalar coupling constants ($^1J_{NH}$ TRIP < $^1J_{NH}$ TiPSY < $^1J_{NH}$ TRIM < $^1J_{NH}$ TRIFP, for details see ESI† Chapter 4) could be reproduced for the *E*-complexes. For the *Z*-complexes, the

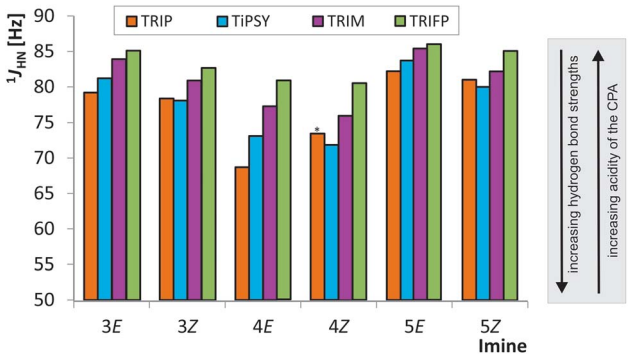

Fig. 4 The experimental CPA/imine $^1J_{HN}$ coupling constants are shown for *E*- and *Z*-imines of **3**, **4** and **5**. The following trend is observed for the *E*-imines: $^1J_{HN}$ TRIP < $^1J_{HN}$ TIPSY < $^1J_{HN}$ TRIM < $^1J_{HN}$ TRIFP. For *Z*-complexes slightly different trend was found: $^1J_{HN}$ TIPSY < $^1J_{HN}$ TRIP < $^1J_{HN}$ TRIM < $^1J_{HN}$ TRIFP. Due to overlap the $^1J_{HN}$ of TRIP/**4** *Z* was determined from HN-HMBC spectra (marked by an asterisk; for all values see ESI† Chapter 3.3).

switched order of TRIP and TiPSY is not reflected in the calculations.

Comparison of internal *vs.* calculated external acidity

Next, the developed internal acidities of the catalysts were compared to experimental and theoretical external acidities. The experimental, external acidities of TRIFP and TRIP as described by O'Donoghue (pK_{aTRIFP} < pK_{aTRIP}) in DMSO,[60] correlate at least in their trend with our internal acidities. Absolute pK_a values of many CPAs in DMSO (SMD) at 298 K using various thermodynamic cycles have been also computed at DFT level of theory.[62] Thus, to compare the internal acidities in DCM at 180 K with the external acidity, we calculated the relative external acidity of TRIP, TRIM and TiPSY to TRIFP (Table 1). In general, the relative external acidities of the investigated CPAs in DCM confirm the previous calculated relative pK_a values in DMSO within ~0.5 pK_a units. This indicates that the implicit solvent model may vary the absolute pK_a values but not the order. Thus, regardless of the choice of dielectric medium, the relative external acidity scale deviates significantly from the internal acidity scale. Especially the almost identical internal acidities of TRIM and TiPSY are not reflected in the calculated external acidities. As a result, this internal acidity scale can be used as a direct experimental indicator for the importance of intermolecular interactions such as dispersion[63,64] in Brønsted acid catalysis, which was already proposed for CPAs and other catalytic systems[65,66] but so far only accessible *via* theoretical calculations/analyses or multicomponent experimental data such as reactivities.[64,67,68]

The presented first internal acidity scale of different CPAs in their binary CPA/imine complexes and to our knowledge the first systematic and broad experimental NMR-study about the trends in hydrogen bond strengths within catalyst/substrate complexes in enantioselective catalysis shows that the intermolecular interactions between catalyst and substrate and potentially also the modulated solvent interactions of the complex significantly affect even the relative acidities. Furthermore, the comparison of the internal with the external acidity may in the future represent a useful tool to evaluate the non-covalent interactions in these complexes and especially the interactions of the 3,3′-substituents, because at least for the imines **3–5** there are common internal acidity trends.

Table 1 Calculated pK_a-values relative to TRIFP in DMSO at 298 K and DCM at 180 K

	$pK_{a,calc}$ in DCM at 180 K (relative to TRIFP)	$pK_{a,calc}$ in DMSO at 298 K (relative to TRIFP)[52]
TRIP	+0.85	+0.55
TRIM	+1.57	+2.26
TiPSY	+6.00	n.a.

Comparison of reactivity and internal acidity

Previously, a correlation was postulated between the acidity of CPAs and their reactivity in a different system. In a Nazarov cyclisation, the highest reactivity was observed for the most acidic CPA catalyst.[44] With the internal CPA acidities at hand, we tested whether this relationship is transferable to the transfer hydrogenation of imines. To compare the internal acidities with reaction rates, the reactivities were determined in CD_2Cl_2.

In the transfer hydrogenation with imine **3** we identified TRIP as the most reactive catalyst. TRIM showed a slightly lower reactivity, followed by TRIFP, while for TiPSY a considerable drop in reactivity was observed (Fig. 5). For the transfer hydrogenation of imine **5** under identical conditions, the order of reactivity is conserved. However, we observed an overall significantly lower reaction rate, which correlated with the Hammett σ_{para} values of the imine aryl substituents (for details see ESI† Chapter 7.3). Obviously, the order of reactivity for the investigated transfer hydrogenation (TRIP > TRIM > TRIFP ≫ TiPSY) does not match the internal acidity scale, which show that TRIP and TiPSY have similar acidities (weakest acids $pK_{aTRIP} \geq pK_{aTiPSY}$ > pK_{aTRIM} > pK_{aTRIFP}). Since the low reactivity of TiPSY (94.6% in the initial linear product build up compared to TRIFP) was already recognized in various reactions, *e.g.* a higher catalyst loading is often necessary, TiPSY might be an exception. Excluding TiPSY, the remaining catalysts TRIP, TRIM and TRIFP show an inverse correlation between reactivity and internal acidity of the catalyst, *i.e.* a direct correlation with H-bond strength.[69] This is in contrast to the previously reported direct correlation with the catalyst acidity in a Nazarov cyclisation.[44]

Reactivity analysis

Next, it was investigated which of the individual steps of the reaction determines the reactivity to obtain a more detailed understanding and to rationalize TiPSY as an outlier.

In general, there are five possible rate-determining steps for the investigated transfer hydrogenation catalytic cycle, all of them potentially affected by the internal acidity: binary complex formation (Fig. 6, step A), *E*- to *Z*-imine isomerization (step B),

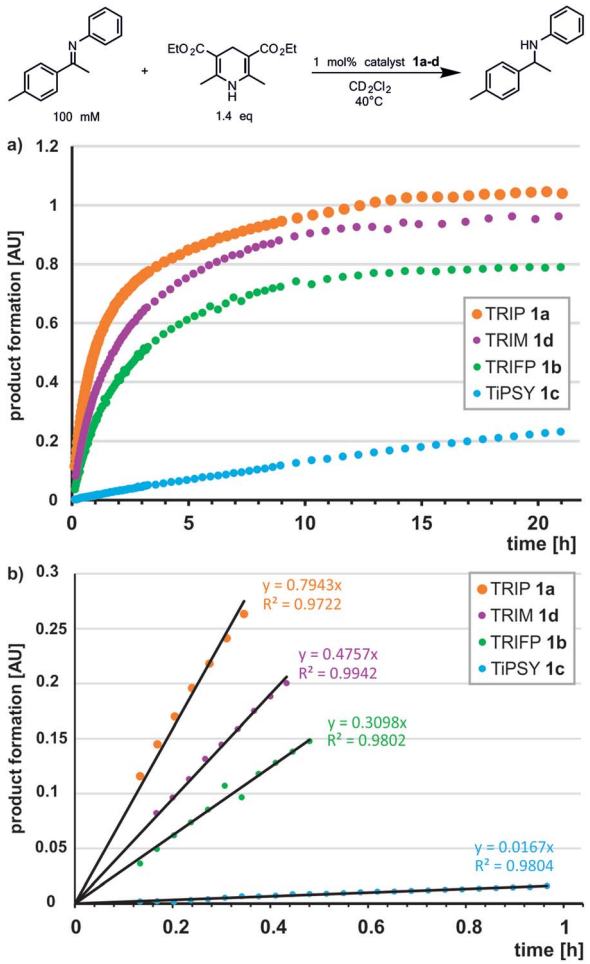

Fig. 5 (a) The reaction profiles for the symmetric transfer hydrogenation of imine **3** were done *in situ* in the NMR spectrometer with 1.4 equivalents of Hantzsch ester and 1 mol% catalyst (TRIP, TRIFP, TiPSY and TRIM) at 40 °C in CD_2Cl_2. (b) The slope of the linear ranges allows to access the rate constants.

formation of the ternary complex (step C), hydride transfer (step D) and product release/product inhibition (step E).

Step A: binary complex formation. The binary complex formation (step A) can be readily observed by mixing the imine and CPA (1 : 1) and directly measuring its NMR spectra. The equilibrium between free imine and imine in the binary complex enables the experimental access to the association constant K_a^b of the binary complex. 1 : 1-samples of the catalysts **1a–1d** and imine **5** show for all catalysts approximately the same amount of free imine (TRIP: 26%, TRIFP: 16%, TRIM: 35% and TiPSY: 27% free imine; for K_a values see Table 2; for spectra see ESI† Chapter 8). The same outcome is observed even with sample preparation at 180 K (see ESI† Chapter 9). At this low temperature condition, no product formation takes place (see ESI† Chapter 10) proving that the binary complex formation ($rate_a^B$) is faster than the observed overall rate ($rate_{obs}$). This indicates a sufficient association constant for this pre-equilibrium (especially at 1 mol% of catalyst, the imine is likely to saturate the catalyst) and suggests kinetics of the binary complex formation not contributing to the rate determining step.

Step B: imine *E*- to *Z* isomerization. The transition state of the hydride transfer originating from the minor-populated *Z*-imine complex has been postulated by calculations and confirmed by our previous studies to be energetically more favoured than that of the *E*-imine complex in this transformation.[21] Hence, after the binary complex formation, the isomerization of the imine may contribute to the rate-determining step (step B). Therefore, we experimentally determined the rate constants of the *E*- to *Z*-isomerization using a combination of low temperature, *in situ* illumination NMR device developed in our group,[70] and photoisomerization. A temperature of 190 K was chosen to suppress thermal back isomerization and thus, upon irradiation with 365 nm, the photostationary states with highest possible *Z*/*E* binary complex ratios between 1 : 1 and 2 : 1 were reached. Next, the temperature was raised to 230 K, the light was switched off, and the decay curves of the thermal *Z*- to *E*-back-isomerization were recorded (for details see ESI† Chapter 11). Fitting of these curves allowed us to obtain the activation barriers for the *Z*- to *E*-isomerization of the binary complexes. From these data and the known Boltzmann distribution of the binary *E*- and *Z*-complexes in the thermodynamic equilibrium (^{1}H spectra), the *E*- to *Z*-isomerization rates were calculated. This experimental access to the isomerization process is independent of the exact mechanism of isomerization (inversion, protonation-rotation and addition-rotation-elimination[71–74]), which may be differently operative dependent on the catalyst.

At 230 K, the experimentally determined isomerization process is fastest for TRIP/**5** ($k_{E\rightarrow Z} = 1.36 \times 10^{-3}$ 1 s^{-1}) and similar for TiPSY/**5** ($k_{E\rightarrow Z} = 5.71 \times 10^{-4}$ 1 s^{-1}) and TRIFP/**5** ($k_{E\rightarrow Z} = 4.45 \times 10^{-4}$ 1 s^{-1}). While the similar offset in the isomerization rates, k_{iso}(TRIP/**5**) : k_{iso}(TRIFP/**5**) = 3.05 and in the observed reaction rate, r_{obs}(TRIP/**5**) : r_{obs}(TRIFP/**5**) = 3.43 fit for TRIP and TRIFP, those for TRIP and TiPSY show a large deviation: k_{iso}(TRIP/**5**) : k_{iso}(TiPSY/**5**) = 2.38 and r_{obs}(TRIP/**5**): r_{obs}(TiPSY/**5**) = 34.33 (see ESI† Chapter 7.3 for reaction kinetic of CPA/**5**). For TRIM such an analysis was not possible due to severe signal overlap. Thus, our results showed that the relative rate of transfer hydrogenation between TRIP and TRIFP is in the same qualitative trend with their relative isomerization rates. However, for the reaction with TiPSY, additional factors may contribute to the steps affecting the overall reaction rate.

Step C: ternary complex formation. The next step in the catalytic cycle is the formation of a ternary complex between CPA, imine and Hantzsch ester (step C) as proposed by theoretical calculations.[11,75–77] Despite extensive efforts in our working group to make the ternary complex accessible by NMR spectroscopy, we have not been able so far to detect any separated proton signals of the ternary complex upon Hantzsch ester addition. For mixtures of TRIP, Hantzsch ester and imine **5** some small changes of chemical shifts were detected (see ESI† Chapter 12), which are most pronounced for the *ortho*-methyl protons of Hantzsch ester and also observable for the hydrogen bond signals of the binary complex. This potentially indicates a fast chemical exchange of the ternary complex formation on the NMR time scale (for spectra see ESI† Chapter 12). Structural

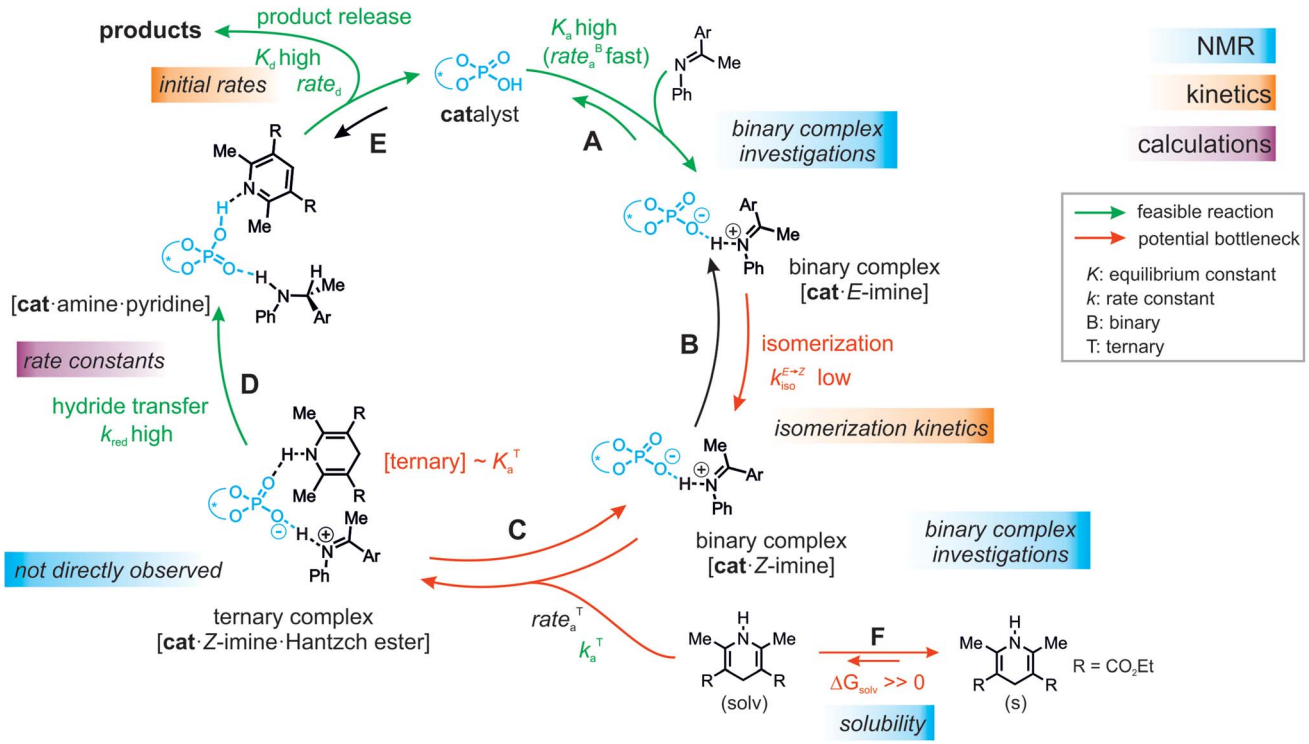

Fig. 6 The catalytic cycle of the investigated transfer hydrogenation of imines is shown. Therefore, all possible rate determining steps are shown. The steps which could be neglected as rate-determining steps by experiments or calculations are shown in green, while the potential bottlenecks are shown in red. Finally, we assume a delicate equilibrium between the *E*- to *Z*-isomerization and the ternary complex formation to be the rate-determining step.

analysis of the computed ternary complex revealed a spatial proximity of the *ortho*-methyl group to the CPA BINOL backbone, which explains the observed high-field shift due to shielding by the aromatic ring (see ESI† Chapter 12 for model structure). For TRIM, under similar conditions no chemical shift changes of the hydrogen bond protons of the binary complex were observed (see ESI† Chapter 13). Thus, the NMR studies of the ternary complex suggests a low (TRIM) to moderate (TRIP) association constant K_a^T and a fast exchange between binary and ternary complex on the NMR time scale even at temperatures down to 180 K, where no reaction occurs.

Additionally, the low solubility of Hantzsch ester (endergonic ΔG_{solv} in step F) in the organic solvents used in this study reduces the concentration of the ternary complex even further and thus amplifies the problem of a low to moderate association constant (K_a^T). Given these experimental results the ternary complex formation/concentration can contribute to the reaction rate or even become the rate determining step and thus influence the relative reactivities of the catalysts. In addition, for a non-isomerizable imine **14**, a 1st order dependence of the dissolved Hantzsch ester concentration on the observed overall reaction rate was found (see ESI† Chapter 7.4). A similar shift of the rate determining step due to concentration modulations has been intentionally used in our previous mechanistic study of dienamines.[78] Assuming the ternary complex formation contributes significantly to the steps determining the overall reaction rate and the solubility of Hantzsch ester is similar in all reactions, the origin of differences in reactivity with various

Table 2 All experimental data discussed above are summarized. Beside the relative, calculated external pK_a values, all experimentally obtained parameters, such as the internal acidity of the CPAs (obtained from ^{15}N chemical shift and $^1J_{NH}$ coupling constant) for both *E*- and *Z*-complexes, the association constants K_a of the binary complexes as well as the *E*- to *Z* isomerisation rates k_{iso} are given. For the sake of completeness also the AREA (θ) values were added.[31] The influence of all these parameters on the relative reaction rate was investigated. TiPSY does not follow the trends observed for the other catalysts TRIP, TRIM and TRIFP (TiPSY is visualized with grey bars)

	external acidity	internal acidity							
		E		*Z*					
	rel. pK_a	$^1J_{NH}$ [Hz]	δ^{15}N [ppm]	$^1J_{NH}$ [Hz]	δ^{15}N [ppm]	K_a [M^{-1}]	$k_{iso}^{E\to Z}$ [10^{-3} s^{-1}]	AREA(θ)	relative reaction rate
TRIP	0.85	82.2	206.6	81.0	209.1	219	1.36	51	47.6
TRIM	1.57	85.4	200.5	82.2	206.0	106	nd	61	28.5
TRIFP	0	86.0	196.4	85.1	204.4	656	0.45	62	18.6
TiPSY	6	83.7	203.6	80.0	211.3	200	0.57	29	1.0
direction of increasing H-bond									

catalysts lies in the alternation of association constant (K_a^T) and/or barrier for the ternary complex formation (k_a^T). Especially the bulkiness of the 3,3′-substituents and their effect on the size of the binding pocket is expected to affect the association constant (K_a^T) and barrier for formation (k_a^T).

Indeed, the AREA (θ) value, a sterical descriptor introduced by Goodman *et al.*, which describes the cone angle of the substrate binding pocket of the CPA is for TiPSY significantly smaller than for the other CPAs.[31] These values (TiPSY: 29°, TRIFP: 62°, TRIM: 61°, TRIP: 51°)[31] demonstrate that the 3,3′-substituents of TiPSY are sterically by far more demanding and may therefore hinder the formation of the ternary complex. Despite the largest sterical hindrance of TiPSY (smallest AREA (θ)), for the binary *Z*-complex the strongest hydrogen bond was found, *i.e.* the formation of the binary complex is not affected by the steric demands of the $SiPh_3$-groups. Thus, the flexibility of the substituents allows the structural adaptation of the catalyst to the imine. This is also corroborated by the experiments, which showed comparable association constants K_a for all catalysts (Table 2). After the binary complex is formed, the degree of freedom of the 3,3′-substituents is reduced in order to maximize the interaction with the imine enthalpically. The structural comparison between TRIP/**3** and TiPSY/**3** revealed a sterical shield for the Hantzsch ester binding for TiPSY/**3**, which indicates a large reorganization penalty (Fig. 7). In contrast, for TRIP/**3** almost no reorganization is required. Thus, the steric of the 3,3′-substituents can explain the large difference in the reactivity of TiPSY compared to the other structurally analogous CPAs.

Step D: hydride transfer. The next step in the catalytic cycle, the hydride transfer (step D) is not accessible by NMR methods. Our calculations for TRIP indicated that the hydride transfer has a by far higher rate constant k_{red} than the isomerization k_{iso} (see ESI† Chapter 14) and can be neglected as the rate-determining step if the ternary complex is formed in a sufficient amount. However, as described above, the marginal ternary complex concentration decelerates the overall rate of the hydride transfer. Therefore, this step is coupled to the ternary complex formation. This is in agreement with the experimentally observed 1st order dependence on the Hantzsch ester concentration for the non-isomerizable imine **14**.

Step E: product release or inhibition. To minimize the potential inhibition of the acidic catalyst by the product basic sites and its effect on the observed reaction rate (step E), we followed the initial rate kinetics approach during our investigations. In this way, product inhibition has a negligible contribution to the rate-determining step in the catalytic cycle. This is most probably valid throughout the course of the reaction. On the contrary, an increase in the reaction turnover with CPA has been reported for the transfer hydrogenation of *N*-methyl imines by protecting the formed highly basic amine. Thus, the *N*-methyl amine was proposed to inhibit the catalyst and leads therefore to a slowdown of the reaction.[79] For our reaction using *N*-phenyl imines, the generated products are unlikely to significantly inhibit the catalytic cycle due to lower basicity of the aromatic amines as evidenced by the high yields. Nevertheless, the initial rate kinetics discussed here avoid the problem of potential product inhibition.

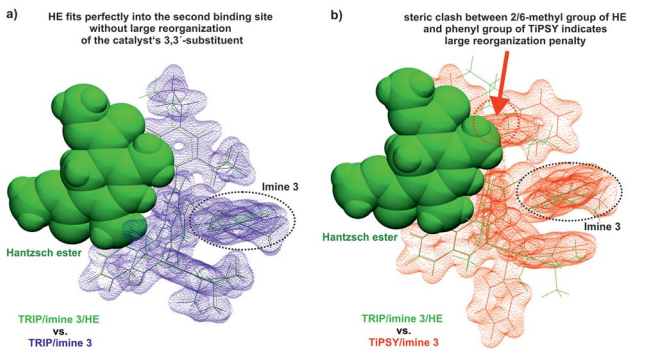

Fig. 7 (a) The comparison of the calculated structures of the binary (blue) and ternary (green) complex with TRIP and imine **3** shows that for the Hantzsch ester (HE) binding almost no reorganization is required. (b) The binary complex of TiPSY and imine **3** (red) revealed a sterical shield for the Hantzsch ester. Thus, before the ternary complex formation, a large reorganization is assumed.

Comprehensive reactivity analysis

All of the experimental data discussed above are summarized in Table 2. Based on the results presented there, a previously established correlation of an increased acidity of the catalyst giving higher reactivity in chiral phosphoric acid-catalysed reactions[44] cannot be transferred to the asymmetric transfer hydrogenation of imines. However, a possible inverse relationship of the internal acidity for TRIP, TRIM and TRIFP with the reactivity could be observed, thus in our system, the less acidic catalysts give the fastest reactions (see Table 2). In contrast, TiPSY does not follow this trend. Despite having the strongest hydrogen bond, as well as a binary complex association constant K_a and an isomerization rate constant k_{iso}, comparable to the other catalysts, the observed reactivity is by far the slowest. The only parameter deviating significantly from the other catalysts is the AREA (θ) value, which is extremely small. In addition, the blockage of the second binding site in TiPSY complexes may amplify the issue of the ternary complex formation within the steps determining the overall reaction rate (see discussion above and Fig. 7). The experimental and theoretical studies on aromatic imines provided, show that the formation of the binary complex as well as product inhibition can be neglected as rate determining steps. Furthermore, the rate constant of hydride transfer (k_{red}) is by far higher than for the isomerization (k_{iso}). Finally, isomerization and ternary complex formation have to be decisive for the observed overall reaction rate. Thus, the comparison of isomerization rates, reaction rates and ternary complex formation of CPAs with different 3,3′-substituents shows that in a delicate equilibrium isomerization rates and ternary complex formation determine the overall reaction rate. Thus, the presented results suggest that within a similar acidic motif and similar sterics of the CPAs the reactivity is inverse correlated to the internal acidity of the catalyst, *i.e.* directly correlated with the H-bond strength in the binary complex. For CPAs with small AREA (θ) values the steric bulk seem to overrule the internal acidity and the reactivity is significantly decreased.

Conclusions

By means of NMR-spectroscopic studies, a hydrogen bond analysis of 32 CPA/imine complexes regarding ^{1}H and ^{15}N chemical shifts as well as $^{1}J_{NH}$ coupling constants was established. This allowed for the first time to implement an internal acidity scale of CPA/imine complexes as a direct experimental tool to probe a correlation between acidity of the catalyst and reactivity. All CPA/imine complexes form strong, charge-assisted hydrogen bonds. The analysis of the chemical shifts and the resulting hydrogen bond strengths of the four Brønsted acid catalysts TRIP, TiPSY, TRIM and TRIFP show two different acidity scales for *E*- and *Z*-imines complexes (*E*-imines: $pK_{aTRIP} > pK_{aTiPSY} > pK_{aTRIM} > pK_{aTRIFP}$; *Z*-imines. $pK_{aTiPSY} > pK_{aTRIP} > pK_{aTRIM} > pK_{aTRIFP}$). All investigated imines showed the same trend. The internal acidity analysis of the CPAs by chemical shifts was corroborated by experimentally determined $^{1}J_{NH}$ coupling constants and theoretical calculations of the complexes. Our calculated external acidity scale in DCM ($pK_{aTRIFP} < pK_{aTRIP} < pK_{aTRIM} < pK_{aTiPSY}$) deviates from the experimental internal acidity scale. This shows that intermolecular interactions in CPA/imine complexes are essential to describe the acidic properties of these complexes correctly and either experimental data or calculations of the binary complexes have to be accounted for.

While the calculated external acidity scale does not exhibit any correlation with the reactivity of the transfer hydrogenation, the internal acidity at least of TRIP, TRIM and TRIFP shows an inverse correlation. Thus, the least acidic TRIP with the strongest hydrogen bond gives the highest reactivity. However, TiPSY does not follow this trend, demonstrating that for Brønsted acids with an identical acidic functional group, also other factors may contribute. Isomerization rates, reaction rates and ternary complex formation data of CPAs with different 3,3′-substituents show that a delicate balance between the isomerization and the ternary complex formation is potentially determining the overall reaction rate. The collected experimental data of TRIP, TRIM and TRIFP suggest that the lower the internal acidity of the catalyst, the higher the isomerization rates and the higher the reactivity in the transfer hydrogenation. This trend can be predicted by calculating internal acidities (*i.e.* $^{1}J_{NH}$ coupling constants), which match the experimental results best. However, for a small binding pocket the correlation with the internal acidities fails, *i.e.* for TiPSY, still a very strong hydrogen bond is formed, but the reactivity breaks down most probably due to sterical congestion at the active site for the second binding partner.

Conflicts of interest

There are no conflicts to declare.

Acknowledgements

Financial Support was provided by the European Research Council (ERC-CoG 614182 – IonPairsAtCatalysis) and intellectual support was provided by SPP 1807 dispersion.

Notes and references

1 M. Terada, *Synthesis*, 2010, 1929–1982.
2 D. Parmar, E. Sugiono, S. Raja and M. Rueping, *Chem. Rev.*, 2014, **114**, 9047–9153.
3 M. Mahlau and B. List, *Angew. Chem., Int. Ed.*, 2013, **52**, 518–533.
4 M. S. Sigman and E. N. Jacobsen, *J. Am. Chem. Soc.*, 1998, **120**, 4901–4902.
5 M. S. Sigman, P. Vachal and E. N. Jacobsen, *Angew. Chem., Int. Ed.*, 2000, **39**, 1279–1281.
6 P. Vachal and E. N. Jacobsen, *J. Am. Chem. Soc.*, 2002, **124**, 10012–10014.
7 T. Akiyama, J. Itoh, K. Yokota and K. Fuchibe, *Angew. Chem., Int. Ed.*, 2004, **43**, 1566–1568.
8 D. Uraguchi and M. Terada, *J. Am. Chem. Soc.*, 2004, **126**, 5356–5357.
9 M. Rueping, T. Theissmann, M. Stoeckel and A. P. Antonchick, *Org. Biomol. Chem.*, 2011, **9**, 6844–6850.
10 Q. Yin, S.-G. Wang and S.-L. You, *Org. Lett.*, 2013, **15**, 2688–2691.
11 T. Marcelli, P. Hammar and F. Himo, *Chem.–Eur. J.*, 2008, **14**, 8562–8571.
12 R. I. Storer, D. E. Carrera, Y. Ni and D. W. C. Macmillan, *J. Am. Chem. Soc.*, 2006, **128**, 84–86.
13 K. Saito and T. Akiyama, *Chem. Commun.*, 2012, **48**, 4573–4575.
14 M. Yamanaka, J. Itoh, K. Fuchibe and T. Akiyama, *J. Am. Chem. Soc.*, 2007, **129**, 6756–6764.
15 X. Xu, Y. Qian, L. Yang and W. Hu, *Chem. Commun.*, 2010, **47**, 797–799.
16 E. P. Ávila, R. M. S. Justo, V. P. Gonçalves, A. A. Pereira, R. Diniz and G. W. Amarante, *J. Org. Chem.*, 2015, **80**, 590–594.
17 K. Shen, X. Liu, Y. Cai, L. Lin and X. Feng, *Chem.–Eur. J.*, 2009, **15**, 6008–6014.
18 M. Rueping, E. Sugiono, C. Azap, T. Theissmann and M. Bolte, *Org. Lett.*, 2005, **7**, 3781–3783.
19 S. Hoffmann, A. M. Seayad and B. List, *Angew. Chem., Int. Ed.*, 2005, **44**, 7424–7427.
20 M. Rueping, C. Azap, E. Sugiono and T. Theissmann, *Synlett*, 2005, 2367–2369.
21 P. Renzi, J. Hioe and R. M. Gschwind, *J. Am. Chem. Soc.*, 2017, **139**, 6752–6760.
22 S. G. Ouellet, A. M. Walji and D. W. C. Macmillan, *Acc. Chem. Res.*, 2007, **40**, 1327–1339.
23 S. Liao, I. Čorić, Q. Wang and B. List, *J. Am. Chem. Soc.*, 2012, **134**, 10765–10768.
24 X. Yu, Y. Wang, G. Wu, H. Song, Z. Zhou and C. Tang, *Eur. J. Inorg. Chem.*, 2011, 3060–3066.
25 Q. Kang, Z.-A. Zhao and S.-L. You, *Org. Lett.*, 2008, **10**, 2031–2034.
26 Q. Gu, Z. Rong, C. Zheng and S. You, *J. Am. Chem. Soc.*, 2010, **132**, 4056–4057.
27 C. Min and D. Seidel, *Chem. Soc. Rev.*, 2017, **46**, 5889–5902.
28 R. Maji, S. C. Mallojjala and S. E. Wheeler, *Chem. Soc. Rev.*, 2018, **47**, 1142–1158.

29 A. J. Neel, A. Milo, M. S. Sigman and F. D. Toste, *J. Am. Chem. Soc.*, 2016, **138**, 3863–3875.
30 M. Orlandi, F. D. Toste and M. S. Sigman, *Angew. Chem., Int. Ed.*, 2017, **56**, 14080–14084.
31 J. P. Reid and J. M. Goodman, *J. Am. Chem. Soc.*, 2016, **138**, 7910–7917.
32 S. E. Wheeler, T. J. Seguin, Y. Guan and A. C. Doney, *Acc. Chem. Res.*, 2016, **49**, 1061–1069.
33 T. J. Seguin and S. E. Wheeler, *Angew. Chem., Int. Ed.*, 2016, **55**, 15889–15893.
34 T. J. Seguin and S. E. Wheeler, *ACS Catal.*, 2016, **6**, 7222–7228.
35 R. Maji, P. A. Champagne, K. N. Houk and S. E. Wheeler, *ACS Catal.*, 2017, **7**, 7332–7339.
36 M. Orlandi, M. J. Hilton, E. Yamamoto, F. D. Toste and M. S. Sigman, *J. Am. Chem. Soc.*, 2017, **139**, 12688–12695.
37 M. Orlandi, J. A. S. Coelho, M. J. Hilton, F. D. Toste and M. S. Sigman, *J. Am. Chem. Soc.*, 2017, **139**, 6803–6806.
38 R. B. Sunoj, *Acc. Chem. Res.*, 2016, **49**, 1019–1028.
39 J. P. Reid and J. M. Goodman, *Chem.–Eur. J.*, 2017, **23**, 14248–14260.
40 F. Duarte and R. S. Paton, *J. Am. Chem. Soc.*, 2017, **139**, 8886–8896.
41 M. Melikian, J. Gramüller, J. Hioe, J. Greindl and R. M. Gschwind, *Chem. Sci.*, 2019, **10**, 5226–5234.
42 N. Sorgenfrei, J. Hioe, J. Greindl, K. Rothermel, F. Morana, N. Lokesh and R. M. Gschwind, *J. Am. Chem. Soc.*, 2016, **138**, 16345–16354.
43 J. Greindl, J. Hioe, N. Sorgenfrei, F. Morana and R. M. Gschwind, *J. Am. Chem. Soc.*, 2016, **138**, 15965–15971.
44 K. Kaupmees, N. Tolstoluzhsky, S. Raja, M. Rueping and I. Leito, *Angew. Chem., Int. Ed.*, 2013, **52**, 11569–11572.
45 M. S. Taylor and E. N. Jacobsen, *Angew. Chem., Int. Ed.*, 2006, **45**, 1520–1543.
46 R. J. Phipps, G. L. Hamilton and F. D. Toste, *Nat. Chem.*, 2012, **4**, 603–614.
47 Q. Zhu, D. E. Graff and R. R. Knowles, *J. Am. Chem. Soc.*, 2018, **140**, 741–747.
48 H. G. Yayla, H. Wang, K. T. Tarantino, H. S. Orbe and R. R. Knowles, *J. Am. Chem. Soc.*, 2016, **138**, 10794–10797.
49 G. Qiu and R. R. Knowles, *J. Am. Chem. Soc.*, 2019, **141**, 2721–2730.
50 K. Gratzer, V. Diemer and J. Clayden, *Org. Biomol. Chem.*, 2017, **15**, 3585–3589.
51 A. Eisenhofer, J. Hioe, R. M. Gschwind and B. König, *Eur. J. Inorg. Chem.*, 2017, 2194–2204.
52 H. Rahaman, Ú. Madarász, I. Pápai and P. M. Pihko, *Angew. Chem., Int. Ed.*, 2011, **50**, 6123–6127.
53 A. J. Neuvonen, T. Földes, Á. Madarász, I. Pápai and P. M. Pihko, *ACS Catal.*, 2017, **7**, 3284–3294.
54 T. Kano and K. Maruoka, *Chem. Commun.*, 2008, 5465–5473.
55 W. Tang, S. Johnston, J. A. Iggo, N. G. Berry, M. Phelan, L. Lian, J. Bacsa and J. Xiao, *Angew. Chem., Int. Ed.*, 2013, **52**, 1668–1672.
56 L. Simón and J. M. Goodman, *J. Am. Chem. Soc.*, 2008, **130**, 8741–8747.
57 H. Benedict, I. G. Shenderovich, O. L. Malkina, V. G. Malkin, G. S. Denisov, N. S. Golubev and H. H. Limbach, *J. Am. Chem. Soc.*, 2000, **122**, 1979–1988.
58 S. Sharif, G. S. Denisov, M. D. Toney and H. H. Limbach, *J. Am. Chem. Soc.*, 2007, **129**, 6313–6327.
59 A. Kuett, I. Leito, I. Kaljurand, L. Soovaeli, V. M. Vlasov, L. M. Yagupolskii and I. A. Koppel, *J. Org. Chem.*, 2006, **71**, 2829–2838.
60 P. Christ, A. G. Lindsay, S. S. Vormittag, J.-M. Neudörfl, A. Berkessel and A. C. O'Donoghue, *Chem.–Eur. J.*, 2011, **17**, 8524–8528.
61 S. Sharif, D. Schagen, M. D. Toney and H.-H. Limbach, *J. Am. Chem. Soc.*, 2007, **129**, 4440–4455.
62 C. Yang, X. S. Xue, J. L. Jin, X. Li and J. P. Cheng, *J. Org. Chem.*, 2013, **78**, 7076–7085.
63 S. Rösel, J. Becker, W. D. Allen and P. R. Schreiner, *J. Am. Chem. Soc.*, 2018, **140**, 14421–14432.
64 J. P. Wagner and P. R. Schreiner, *Angew. Chem., Int. Ed.*, 2015, **54**, 12274–12296.
65 R. Y. Liu, S. L. Buchwald, P. Liu, Y. Yang, G. Lu, D. S. Lambrecht and C. Fang, *J. Am. Chem. Soc.*, 2017, **139**, 16548–16555.
66 X. Cai, A. Tohti, C. Ramirez, H. Harb, J. C. Fettinger, H. P. Hratchian and B. J. Stokes, *Org. Lett.*, 2019, **21**, 1574–1577.
67 D. Seebach, U. Groselj and W. B. Schweizer, *Helv. Chim. Acta*, 2010, **93**, 1–16.
68 A. Armstrong, R. A. Boto, P. Dingwall, J. Contreras-García, M. J. Harvey, N. J. Mason and H. S. Rzepa, *Chem. Sci.*, 2014, **5**, 2057–2071.
69 No absolute correlation between ee values and H-bond strength/internal acidity was identified. Relative correlations are under current investigation.
70 C. Feldmeier, H. Bartling, E. Riedle and R. M. Gschwind, *J. Magn. Reson.*, 2013, **232**, 39–44.
71 C. H. Bushweller, J. W. O'Neil and H. S. Bilofsky, *Tetrahedron*, 1971, **27**, 5761–5766.
72 C. H. Bushweller, J. W. O'Neil and H. S. Bilofsky, *J. Am. Chem. Soc.*, 1970, **92**, 6349–6350.
73 M. I. Rodríguez-Franco, I. Dorronsoro, A. Castro and A. Martínez, *Tetrahedron*, 2000, **56**, 1739–1743.
74 M. Dewar and B. Jennings, *Tetrahedron Lett.*, 1970, **11**, 339–342.
75 L. Simón and J. M. Goodman, *J. Am. Chem. Soc.*, 2008, **130**, 8741–8747.
76 L. Simón and J. M. Goodman, *J. Org. Chem.*, 2011, **76**, 1775–1788.
77 J. P. Reid, L. Simón and J. M. Goodman, *Acc. Chem. Res.*, 2016, **49**, 1029–1041.
78 A. Seegerer, J. Hioe, M. M. Hammer, F. Morana, P. J. W. Fuchs and R. M. Gschwind, *J. Am. Chem. Soc.*, 2016, **138**, 9864–9873.
79 V. N. Wakchaure, P. S. J. Kaib, M. Leutzsch and B. List, *Angew. Chem., Int. Ed.*, 2015, **54**, 11852–11856.